

THE LIFECYCLE OF INTERSTELLAR DUST AS CONSTRAINED BY NOBLE GAS IMPLANTATION INTO SiC GRAINS

P. Guillard¹, A. P. Jones¹ and A.G.G.M Tielens²

Abstract. Primitive meteorites contain presolar grains that originated in stellar outflows and supernovae ejecta prior to the formation of the solar system. These grains represent a unique means to access interstellar matter within the framework of dust evolution. Laboratory measurements of the noble gas abundances trapped into a large sample of presolar SiC grains recovered from the Murchison meteorite showed a strong enrichment of the heavier gases (Xe, Kr) compared to the lighter ones (He, Ne, Ar) for both solar (so-called *N*) and Asymptotic Giant Branch (AGB)-star (so-called *G*) isotopic components isolated from SiC. This cannot possibly be due to nuclear processes, but requires some fractionation process.

We have developed a simple atom implantation and grain erosion model which allows us to better understand this mass-fractionation of the elemental abundances and which provides new insights on both the physical conditions of grain formation and implantation around evolved stars and the processing of dust in circumstellar and interstellar environments. We argue in favor of an implantation at constant gas-grain velocity so that heavier elements are implanted more deeply, and thus are more susceptible to be conserved during erosion in the interstellar medium (ISM).

We show that the *N*-component has been implanted in supernova-generated shock waves in the ISM, at a relatively low velocity ($120 \pm 40 \text{ km s}^{-1}$) and high equivalent hydrogen-fluences (10^{18} to 10^{19} cm^{-2}) in a so-called *steady-state* regime where implantation is accompanied by erosion. On the other hand, the *G*-component is consistent with implantation in the fast ($220 \pm 20 \text{ km s}^{-1}$) wind of the planetary nebulae (PN) phase, at low H-fluences (10^{17} to 10^{18} cm^{-2}) so that one can ignore erosion at this stage. In both cases, the mass-driven fractionation of the observed elemental abundances is a result of implantation in different astrophysical sites and subsequent erosion mainly in the ISM.

1 Introduction

Primitive meteorites exhibit components with anomalous isotopic compositions with respect to their bulk composition, generally assumed to be solar. These isotopic anomalies are characteristic of various nucleosynthetic processes in red giants and supernovae, which indicates that identified pre-solar dust components (including silicon carbide, nano-diamonds and graphite) primarily originate from the circumstellar ejecta of evolved stellar objects (see e.g. Anders & Zinner 1993 for a comprehensive review of this subject). This led to the notion that pre-solar grains have thus survived processing in the ISM, the formation of the solar nebula and incorporation into the forming planets or asteroids, without completely losing their identity.

Models of stellar nucleosynthesis of the elements have come to rely heavily on the isotopic and elemental ratios that have been measured in interstellar silicon carbide (SiC) grains recovered from meteorites (Lewis et al. 1990, 1994). The strong enrichment of the heavier elements cannot possibly be due to nuclear processes (Lewis et al. 1994; Heck et al. 2007), but requires some fractionation process. Before the wealth of data locked up in the stardust can be interpreted, the effects of ion implantation as well as grain processing in the solar nebula, and in interstellar and circumstellar media, must be fully understood.

We focus here on understanding the global trends in the measured noble gas abundances in SiC grains, and particularly the fractionation of the lighter noble gases relative to the heavier ones. This study is restricted to the following noble gas atoms: ^4He , ^{22}Ne , ^{36}Ar , ^{82}Kr and ^{130}Xe . In this paper we present the main results of a model

¹ Institut d'Astrophysique Spatiale (IAS), Université Paris Sud, Bât. 121, 91405 Orsay Cedex, France

² NASA Ames Research Center, Mail Stop 245-3, Moffett Field, CA 94035, USA

that takes into account dust processing (mainly sputtering) which follows or accompanies ion implantation. We consider that this mass-fractionation provides important clues to the physical processes driving dust evolution and the history of the recovered grains. These interpretations assume that the chemical treatments used to extract grains from the bulk meteorite do not much affect the SiC grains. This hypothesis is confirmed by in situ studies of SiC grains which show that properties (grain size distribution, surface morphology, shape, etc) of these grains were the same that extracted ones (Bernatowicz et al. 1996).

2 Noble gases in SiC meteoritic grains

2.1 The mass fractionation in the laboratory data

Two distinct noble gas components can be separated from the SiC grains. The so-called *G*-component shows isotopic ratios that are characteristic of the s-process taking place in the He-shell of AGB stars (Lewis et al. 1990, 1994; Gallino et al. 1990; Alexander 1993). The *N*-component, with near but not necessarily exactly solar system isotopic abundances, is often thought to represent stellar envelope material. However, we propose that it is mainly a relic of implantation in the ISM during supernovae-generated shocks because the low relative gas-grain velocities in the AGB shell ($\sim 10 \text{ km s}^{-1}$) imply very shallow implantation depths of order only a few Å, so that these elements would rather be easily lost from the grains.

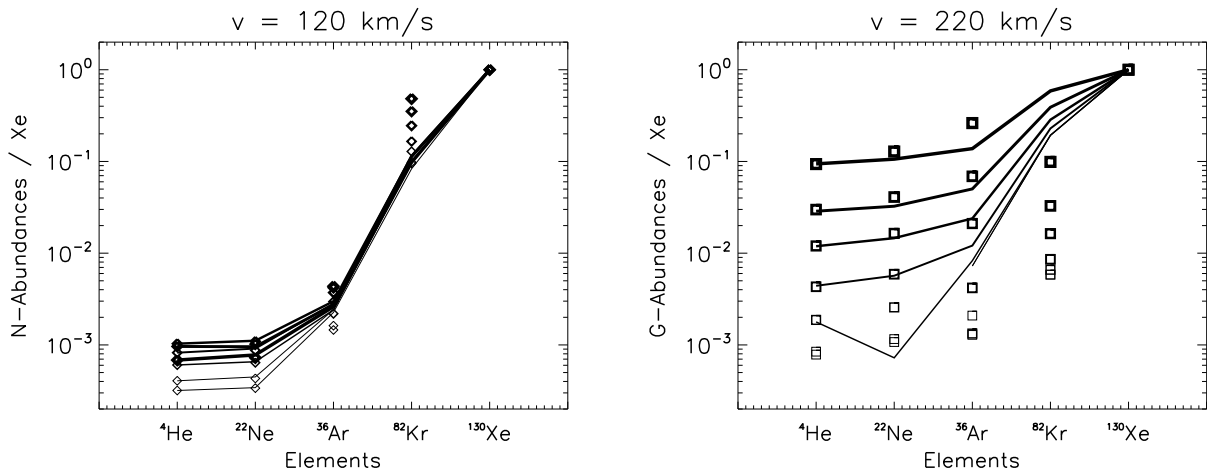


Fig. 1. Implanted noble gas abundances in the SiC grains extracted from the Murchison meteorite for the *N*- (Left) and *G*- (Right) components. The elemental abundances have been normalized to ^{130}Xe and to Solar abundances for *N* or AGB abundances for *G*. Each symbol represents a given SiC grain size fraction, thicker lines denoting bigger grains. Error bars are smaller than the symbols. The superimposed lines show the abundances computed from the model (see sect. 4) for the *steady-state* (*N*) and *post-implantation erosion* (*G*) regimes, respectively. The implantation velocities derived from the model are given at the top of each plot.

The points in Fig. 1 show the elemental abundances of the noble gases separated into their *N*- and *G*-components, normalised to the respective reference abundances (solar for *N* and AGB for *G*) and to that of Xe. The SiC samples were separated into several size fractions (7 size-bins from 0.19 to 1.51 μm in radius), corresponding to the different points for one given element (Fig. 1). In contrast to Lewis et al. (1990, 1994), we have elected to normalize the abundances to that of Xe rather than He because we attribute the observed fractionation pattern to loss of the lighter elements relative to the heavier ones. Thus, Xe atoms best represent the implanted species, because they are the most deeply implanted and therefore the best preserved in the grains.

Examining the general trend (Fig. 1), the data clearly indicate a strong enrichment of the heavier atoms, which is still not fully understood. Here we propose a simple explanation: the observed trend in the mass fractionation between the different noble gases is due to the process of implantation at constant gas-grain

velocity (inertial regime¹) and the loss of elements during erosion, mainly during shock-processing in the ISM. On the contrary, thermal implantation (with equal energies for all elements) would lead to a fractionation pattern showing an increase in the abundance of the lighter elements relative to the heavier ones. For the bigger grains, which represents the most reliable data and the case where our model is more robust (see § 3), the *G*-component is less fractionated relative to its source (i.e. the ratios Kr/Ar, Ar/Ne, Ne/He are approximately constant) compared to the *N* component. Therefore, the *G*-component must have been implanted deeper into the grain, i.e. at *higher velocities*, than the *N*-component.

Moreover, we note that the fractionation for each component is size dependent, with the fractionation being most severe for the smaller grains and with a stronger size-dependence for the *G*-component. The modelling of these effects are beyond the scope of the paper and will not be treated here (see Guillard et al. 2007 for more details).

2.2 Equivalent H-Fluences seen by interstellar grains

We have converted the noble gases concentrations measured by Lewis et al. (1990, 1994) to the equivalent H-fluences, i.e. the number of H-atoms per unit cross section that the grains were exposed to. These fluences are shown on Fig. 2 for both *N* and *G*-components as a function of the grain radius.

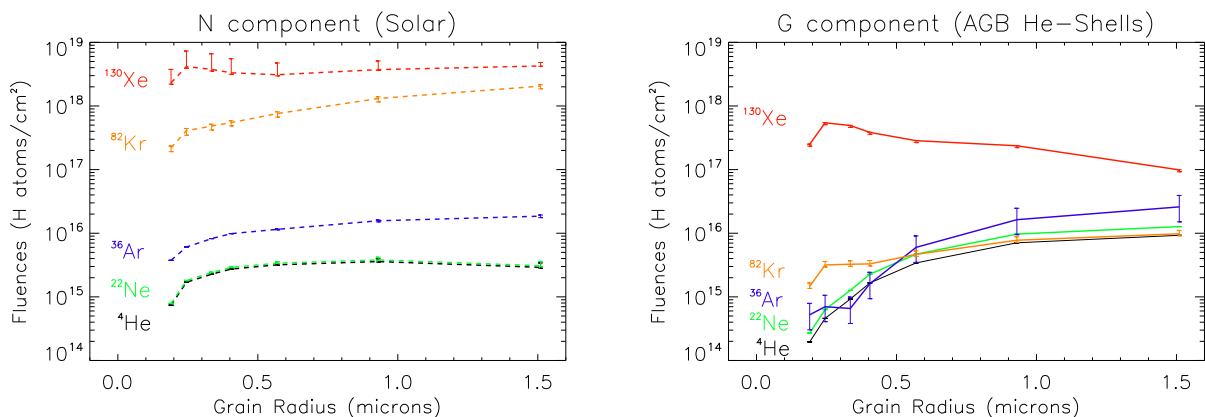


Fig. 2. Implied H atom fluences derived from the noble gas atom data by normalization to unit grain cross sections and to the relevant abundances, i.e. AGB He-Shell for the *G* component (right) and Solar for the *N* component (left). The error bars take into account the range of abundances for AGB-star He Shells.

As obvious from the fractionation pattern discussed before, the Xe atom data, which is the best-preserved implanted species, indicates the highest equivalent H-fluences: 10^{18} to 10^{19} cm^{-2} for the *N*-component and 10^{17} to 10^{18} cm^{-2} for the *G*-component. Indeed, taken at face value, the He data implies a fluence of only 10^{15} cm^{-2} (Lewis et al. 1994). For the *N*-component, the derived fluences are relatively independent of grain size with only a slight decrease for the smallest sizes (radii $a < 1 \mu\text{m}$). The size-dependence is more pronounced for the *G*-component. It should be born in mind that these derived fluences are only lower limits because some fraction of the implanted noble gasses will have been removed during processing in the solar nebula and in the interstellar medium. Moreover, the noble gases may be concentrated in a subset of the grains analysed (Lewis et al. 1990, 1994).

The equivalent H-fluences derived for the *N* component are strikingly consistent with those seen by a grain in a *typical interstellar shock* (10^{18} to 10^{19} cm^{-2} , see Jones 1994, 1996). In addition, the high fractionation measured for the *N* component is consistent with implantation at lower energies (i.e. shallow) but at high fluence (i.e. where loss due to surface sputtering is important) by a non-thermal process behind interstellar shock waves (see sect. 4).

¹a regime where the grains interact with a wind of a constant velocity

v [km/s]	He				Xe			
	E [keV]	R_p [Å]	ΔR_p [Å]	S_k	E [keV]	R_p [Å]	ΔR_p [Å]	S_k
100	0.208	11.3	13.4	0.108	6.78	73.3	19.9	0.387
400	3.336	197.7	127.3	-0.368	108.41	377.7	100.5	0.322
1000	20.848	1236.4	418.5	-1.228	677.56	1793.5	441.3	0.048

Table 1. Example values of implantation parameters (energy, E , mean implantation depth, R_p , implantation distribution width, ΔR_p , and skewness, S_k) for He and Xe noble gas into SiC as a function of impact velocity. Note the sign change in the skewness S_k for He, which is also visible on the forms of the profiles (Fig. 3).

3 A model of ion implantation and dust grain erosion

3.1 Implantation profiles

Because of their importance in electronics and their applications as inner linings in Tokomaks, ion implantation and erosion of SiC have been well studied experimentally (see e.g. Burenkov 1986; Behrish 1991; Gnaser 1999). The measured ion implantation profiles have been successfully matched by skewed gaussian distribution functions, known as Pearson distributions. The implanted species distribution profile in a semi-infinite slab is determined by three parameters (spatial moments of the statistical functions): the average projected range R_p , the mean square range straggling ΔR_p , which measures the width of the implantation profile, and the skewness S_k (asymmetry parameter). These parameters depend on the incident atom, its energy, the geometry impact, and the nature of the substrate.

By means of 2-D interpolations we have determined the statistical parameters describing the implantation profiles for a relevant range of impact velocities (0 to 1000 km s⁻¹). All but the Xe ion data were available (Burenkov, 1986), so for the latter we have used the antimony, Sb, ion data which is close in mass and is therefore a good approximation. The results are given in Table 1 and Fig. 3. The shape and position of these profiles provides constraints on the mass fractionation measured in the presolar SiC grains. The lighter elements will be more fractionated relative to the heavier ones and this fractionation is more pronounced if the initial implantation occurs at relatively low velocity (small implantation depth). As an example, erosion of a 40 Å layer from a grain implanted at 100 km s⁻¹ removes most of the He but very little Xe. On the contrary, erosion of a 40 Å layer from a grain implanted at 400 km s⁻¹ will only cause weak He fractionation relative to Xe.

We successfully compared our implantation ranges to SRIM² simulations. The use of semi-infinite slab implantation profiles is justified because the grain diameter is large compared to the implantation range. We found that the loss of ions through the surface is unimportant in this study. Indeed, at the considered velocities (< 300 km s⁻¹), the implantation depths (maximum 0.05 μm) are much smaller than the grain radii, even for the smaller grains (0.38 μm). We performed SRIM simulations and computed the fractions of ions that escape from our spherical grains: for the velocities (~ 100 km s⁻¹ and 200 km s⁻¹) and the energies that we consider, this fraction is negligible (about 0.002 % for the highest velocity and for Xe). Thus, the incident atoms did not traverse the grains. Moreover, we do not consider the deflection of the particle from its linear implantation trajectory. But this phenomenon is only important for small spherical grains and near tangential implantation into the grain.

3.2 Erosion of SiC dust grains and implantation regimes

Sputtering will occur where there is a large differential velocity (> 30 km s⁻¹, Tielens et al. 1994) between the gas and the grains, for example, due to radiation pressure, stellar winds, ion acceleration in magnetic fields, or shock waves. Schematically, we distinguish two limiting physical regimes for implantation/erosion. First, surface erosion during the implantation is neglected and erosion takes place separately and subsequently to the implantation (so-called *post-implantation erosion regime*). Physically, it is the case for low-fluence implantation ($D < 10^{18}$ cm⁻²). Guillard et al. (2007) showed that it is characteristic of the *G*-component. On the other hand, i.e. for high-fluence ion implantation (*N*-component), the destruction by sputtering is accompanied by

²SRIM is a group of programs which calculate the stopping and range of ions (up to 2 GeV/amu) into matter using Monte Carlo simulations and a quantum mechanical treatment of ion-atom collisions (see Ziegler 1985 and <http://www.srim.org/>)

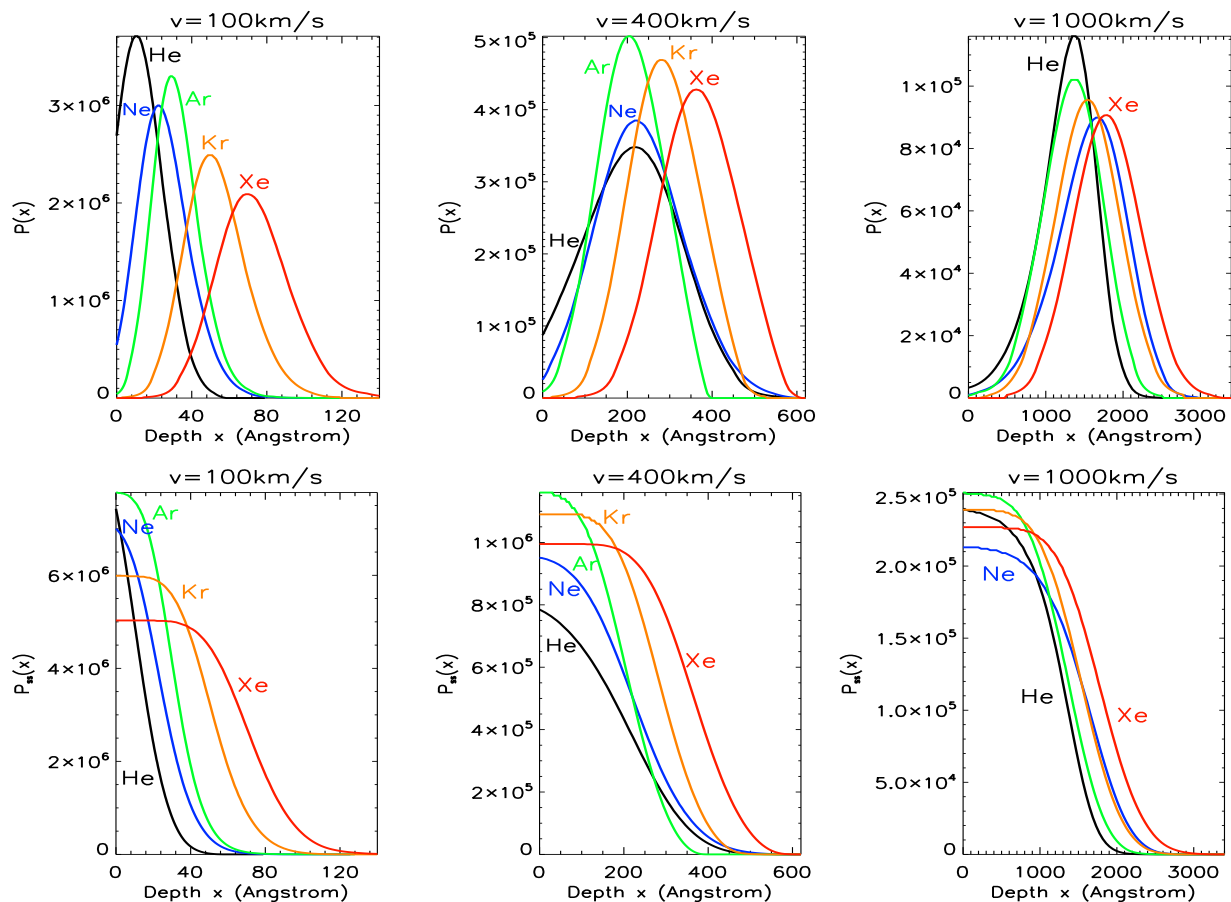


Fig. 3. Noble gas implantation profiles for the two implantation/erosion regimes (top: post-implantation erosion; bottom: steady-state). The number of implanted ions per unit depth is given as a function of implantation depth for 3 ion-grain relative velocities (100, 400 and 1000 km s⁻¹).

fresh implantation (e.g. Whestphal & Bradley 2004). In this case, the implantation profile of each species will evolve towards a steady state, balancing implantation with surface loss due to erosion (see Fig. 3).

4 Fractionation model results and astrophysical implications

Taking into account these two implantation regimes (post-implantation erosion for G and steady-state for N), we computed the elemental abundances of the noble gases trapped into the grains as a function of the eroded depth. We then determine which eroded depth is necessary to reproduce the He fractionation. Finally, given the implantation profiles, we use this eroded depth to compute the elemental abundances of the other elements.

The results of this fractionation model are given in Fig. 1. The symbols (diamonds for N and squares for the G -component) represent the data. The calculated abundances from the model (*post-implantation erosion* for G and *steady-state* regime for N) are the points linked the lines (of variable thickness to represent the grain sizes). We only show the results for the optimum implantation velocities. Further results are given in Guillard et al. 2007. A precise treatment of implantation and erosion into small spherical grains is not included in this model³, which explains why the small grains data and the size-dependence of the fractionation are not well reproduced (especially for the Kr data). However, our model explains the global fractionation trends between light and

³A more quantitative analysis of the size-dependence requires detailed grain trajectory calculations relevant for interstellar shocks (see Slavin et al. 2004, Guillet et al. 2007). This is beyond the scope of this paper, and we are currently extending our work in this direction.

heavy noble gases well for larger grains and both components. For the G -component, the model reproduces the measured fractionation trends well for a rather narrow range of velocities: $v_{imp}^{(G)} = 220 \pm 20 \text{ km s}^{-1}$. For the N -component a global agreement between the data and the modeled abundances (for the steady-state implantation/erosion regime) is obtained for a somewhat wider range of velocities than for the G -component, i.e. $v_{imp}^{(N)} = 120 \pm 40 \text{ km s}^{-1}$.

In order to further constrain the astrophysical sites where dust implantation/erosion take place, we checked if our inferred eroded depths are compatible with those given by yields calculations (see Tielens et al. 1994) or by interstellar shock models (Jones et al. 1996; Slavin et al. 2004). The results show that the recovered grains have, on average, been exposed to at least two $\sim 100 \text{ km s}^{-1}$ interstellar shocks, which is statistically consistent with the grain lifetimes ($\sim 100 \text{ Myr}$) and supernova rate for the Galaxy. Since shocks removed the previously shallow-implanted species, it is likely that the grains only record the effect of the fastest shock that they have experienced.

These considerations lead us to propose the following general scenario: the G -component was implanted with He shell material in the fast wind of the PN phase at low fluence and high gas-grain velocity ($\sim 200 \text{ km s}^{-1}$), accompanied by very little erosion, and then subsequently injected into the ISM and eroded by sputtering in interstellar shocks (at least 2), not only leading to a preferential removal of the lighter, less-deeply implanted noble gases but also to the implantation of the N -component itself. The N -component is indeed attributed to inertial, steady-state implantation, with accompanying erosion, at high fluences and lower velocities behind interstellar shocks. The lower energies combined with the higher fluences in this environment (as compared to planetary nebulae) then lead to more pronounced fractionation during the implantation process itself.

5 Conclusions and perspectives for future instruments

In interpreting the laboratory data of Lewis et al. (1990, 1994) through the use of simple implantation models we have been able to better understand the characteristics of the implantation process and to constrain the astrophysical conditions in the implantation/erosion sites. The fractionation of the noble gases by mass, in both the N and G -components, is consistent with implantation before (G) or during (N) sputtering in the interstellar medium, and is also consistent with the inferred exposure ages of the SiC grains in the interstellar medium ($\sim 100 \text{ Myr}$).

These studies need to be followed-up with incoming instruments. The Planck satellite and ALMA (Atacama Large Millimeter Array) interferometer will allow to access to the properties of the dust injected by stars in the ISM and determine the contribution of AGB stars to the galactic dust budget. The Herschel satellite will provide us with a unique view of shock-processed dust which will be fundamental to understand the nature and location of the physical processes that drives dust evolution.

References

- Alexander, C. M. O. 1993, *GeCoA*, 57, 2869
- Anders, E. & Zinner, E. 1993, *Meteoritics*, 28, 490
- Bernatowicz, T. J. et al. 1996, *ApJ*, 472, 760
- Burenkov, A. F. et al. 1986, *Tables of ion implantation spatial distributions*
- Berisch, R. 1991, *Sputtering by particle bombardment III*
- Gallino, R. et al. 1990, *Nature*, 348, 298
- Gnaser, H. 1999, *Low Energy Ion irradiation of solid surfaces*
- Guillard, P., Jones, A.P. & Tielens, A. G. G. M., 2007, *A&A*, submitted
- Guillet, V., Pineau des Forêts, G., Jones, A.P., 2007, *A&A*, in press
- Heck, P. R. et al. 2007, *ApJ*, 656, 1208
- Jones, A. P. et al. 1996, *ApJ*, 469, 740
- Jones, A. P. et al. 1994, *ApJ*, 433, 797
- Lewis, R. S., Amari, S. & Anders, E. 1990, *Nature*, 348, 293
- Lewis, R. S., Amari, S. & Anders, E. 1994, *GeCoA*, 58, 471
- Slavin, J. D., Jones, A. P., & Tielens, A. G. G. M. 2004, *ApJ*, 614, 796
- Tielens, A. G. G. M. et al. 1994, 431, 321
- Westphal, A. J. & Bradley, J. P. 2004, *ApJ*, 617, 1131